JOURNAL OF MATERIALS SCIENCE 26 (1991) 2615–2620

Damage mechanisms of fatigue fracture in a metastable beta Ti–15–3 alloy

I. MOSTAFA*, G. WELSCH*, A. MOET‡
*Departments of Materials Science and Engineering and ‡Macromolecular Science, Case Western Reserve University, Cleveland, Ohio 44016, USA

The mechanism of crack tip deformation in metastable beta Ti–15–3 alloy under fatigue loading has been examined. In spite of the small thickness of the test specimens (1 mm), the plastic zone revealed plane strain conditions which was transformed to a plane stress zone when its size became 0.25 of the crack length. Slip processes whose density increased with crack length were the dominant microscopic feature of crack tip plasticity. Microcracks emanating from the main crack appeared as a result of extensive slip damage. Transmission electron microscopy (TEM) and X-ray evidence indicate the absence of twinning or phase transformation and that dislocation processes constitute the microstructural origin of crack propagation resistance in the alloy. Energy calculations show that the specific energy of slip, 20 MJ m^{-3}, exceeds that of microcracking by three orders of magnitude.

1. Introduction

The magnitude and the type of crack tip damage in a material determines its resistance to crack propagation. This phenomenon is commonly modelled as a plastic zone and is analysed according to principles of nonlinear fracture mechanics [1–5]. When damage processes are highly localized in the crack tip region, a process zone model is invoked [6, 7]. The latter rests on linear elastic fracture mechanics. Both approaches regard crack tip damage in a continuum sense. However, advanced analysis of deformation processes reveals that plasticity is a continuum manifestation of various microstructural transformation such as dislocation slips, twinning and phase transformation [8–12].

Each of these processes requires differing energy expenditure, hence the influence of each on resisting crack advance should be different. Furthermore, the density of their occurrence should play an equally significant role. Accordingly, a complete characterization of a material's fracture toughness demands a careful examination of the type and the evolution of the crack tip damage processes during its propagation. This paper reports a detailed examination of fatigue crack tip damage mechanisms in a metastable beta Ti–15–3 alloy.

2. Experimental procedure

2.1. Fatigue tests

Single edge notched (SEN) specimens were prepared from 1 mm thick Ti–15–3 alloy sheets. All the specimens had their longitudinal axis parallel to the rolling direction in order to maintain identical texture conditions. The gauge dimensions of the specimens were 80 mm × 20 mm with a 60 degree, 1 mm deep notch introduced into one edge of each specimen. The surfaces of the specimens were polished mechanically, using 0.3 μm aluminium oxide powder in the final polishing step to obtain mirror-like surface quality. This quality is needed in order to conduct optical observations on the damage zone during and after fatigue tests. The specimens were fatigued at room temperature using a servo-hydraulic MTS machine. The maximum load in the fatigue cycles was kept constant at 380 MPa which corresponds to 50% of the yield strength of the alloy. The load cycling frequency was 0.5 Hz with a sinusoidal waveform. The minimum to the maximum load ratio was 0.1.

Two sets of specimens were tested. One set was fatigued until complete fracture occurred. This set was used for the analysis of the evolution of crack tip damage zone. The second set was fatigued to certain crack lengths and unloaded. These cracked, yet unfractured, specimens were used to investigate the crack tip damage mechanisms. Similar mechanistic investigations were also performed on fractured specimens. Microscopic analyses were made with a Nikon-AFX-II optical microscope and a Jeol 35 CF scanning electron microscope (SEM).

2.2. X-ray diffraction analysis

Samples used for X-ray diffraction (XRD) analysis were cut from as-received material as well as from the damage zones of propagating cracks (Fig. 1a and b). The lengths of these cracks were 4 mm and 8 mm while the critical crack length under our test conditions was 12 mm. The size of the samples was 2 mm × 2 mm × 1 mm. X-ray diffraction analyses were performed on a Philips diffractometer system ADP 3520, with nickel-filtered Cu$K\alpha$ monochromatic radiation.

0022–2461/91 $03.00 + .12

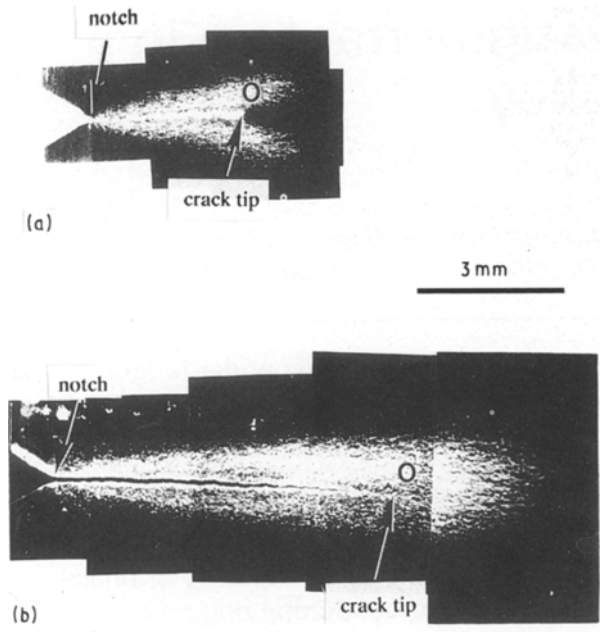

Figure 1 Optical micrograph of the side view of (a) 4 mm crack length displaying the V-shape of the damage zone and (b) 8 mm crack length displaying the circular shape of the damage zone. The circle indicates the area at which X-ray and TEM analyses were carried out.

2.3. Transmission electron microscopy analysis

Samples used for TEM analysis were removed from the same locations shown in Fig. 1a and b, as well as from as-received material. These samples were carefully ground to about 0.1 mm thickness on a grinding wheel with 600 mesh emery papers. Then, discettes with 3 mm diameter were punched out from the specimens. The discettes were further thinned using a Struer Tenupol twin-jet electropolishing system. In such a system, the polishing current was automatically cut off as soon as a small hole formed in the polished discette. The electropolishing solution was 6% perchloric acid, 35% butanol n-butyl alcohol and 59% methanol by volume. The solution temperature was kept at $-40\,^{\circ}C$, the current density was 15 mA mm^{-2} and the voltage was 25 V. After polishing, the TEM foils were washed in methanol prior to TEM examination. That examination was performed on a Philips 400T TEM.

3. Results and discussion

3.1. Evolution of the crack tip damage zone

Results of this study are presented in three statements. The first deals with the evolution of the crack tip damage as a continuum, i.e., plastic zone as a function of crack advance. The second examines the structural origin of the damage processes. In the third statement, an energy analysis is carried out to assess the specific energy of the identified damage processes. In a subsequent publication, we employ the Crack Layer theory to evaluate the specific energy of fracture [13] which will be compared with the present results.

The shapes of the crack tip damage zone which are displayed in Fig. 1a and b are typically observed at short and long cracks, respectively. With crack growth, that zone experienced shape change and its size increased. In the early stages of crack propagation, the damage zone had a V-shaped (Fig. 1a). As the crack propagated, a gradual merge of the two edges of the damage zone caused it to assume a circular leading edge (Fig. 1b). The crack propagated preceded by the circular front of the damage zone till the final rupture.

Obviously, the shape change of the damage zone reflects a gradual change in the stress state with crack depth. At short crack, plane strain conditions prevailed, giving rise to the V-shape of the damage zone. Subsequently, plane stress conditions prevailed with the increase of the crack depth exhibiting the circular shape of the damage zone [14].

Plastic deformation process during crack propagation caused lateral contraction due to yielding within the damage zone. The extent of yielding increased with the crack length. Fig. 2 is a composite micrograph of one half of a fatigue-broken specimen. In the beginning, the crack propagates through a plane normal to the applied load as is evident from the flat appearance of the fracture surface. This region coincides with plane strain conditions. As the crack is dominated by plane stress, it propagated in a plane that slanted. These phenomena can be better examined from cross-sections of fractured specimen. Fig. 3a–d are optical micrographs of cross-sections at 3, 6, 9 and 12 mm crack length, respectively. There is no noticeable thickness reduction or fracture surface slanting at short crack (Fig. 3a). However, with crack propagation the magnitude of fracture surface yielding as well as slanting increased remarkably (Fig. 3b and c). At the critical crack length, the specimen fractured in the loading portion of fatigue cycle showing a fracture surface similar to that created under monotonic loading (Fig. 3d). It should be noted, however, that the progressive slanting of the fracture surface is an additional indication of the stress state change at the crack tip, from plane strain to plane stress [15]. In spite of the fact that fatigue tests were performed on 1 mm thick specimen, yet the plane strain conditions prevailed at the tip of short crack.

It is worth noting that the maximum thickness reduction took place at the fracture surface. This reflects the maximum yielding strain in the damage zone preceding the crack tip. The thickness t at the

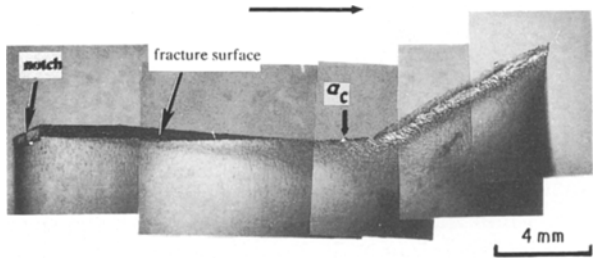

Figure 2 A composite optical micrograph of one half of fatigue-broken specimen showing the yielding as well as the slanting of the fracture surface.

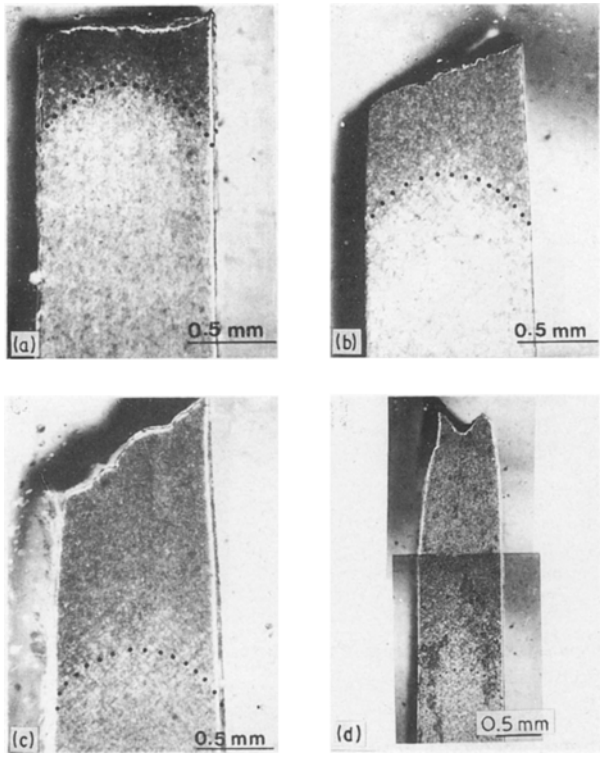

Figure 3 Cross-section of the specimen shown in Fig. 2 at (a) 3, (b) 6, (c) 9 and (d) 12 mm crack length.

fracture surface was measured for different crack increments and normalized to the initial specimen thickness t_0. The normalized thickness t/t_0 was taken as a measure of the maximum yielding of the crack tip damage zone and was plotted as a function of the crack length in Fig. 4. The local yielding seems unnoticeable during the first millimetre of the crack propagation. Beyond this length yielding increased at a steady rate reaching 50% at the critical crack length.

Fig. 5 is a composite micrograph of the side view of two halves of a fractured specimen. The width of the damage zone increased about eight-fold from crack initiation to the critical crack length marked by a_c. The damage features do not cover the entire damage zone as they appear in Fig. 1. A close up of different regions along the crack trajectory shows that the damage process involves discrete microstructural discontinuities. Surface traces (due to dislocation slips and/or twinning) and secondary cracking are evident along the primary crack path as shown in Fig. 5. The density of the surface traces increased remarkably

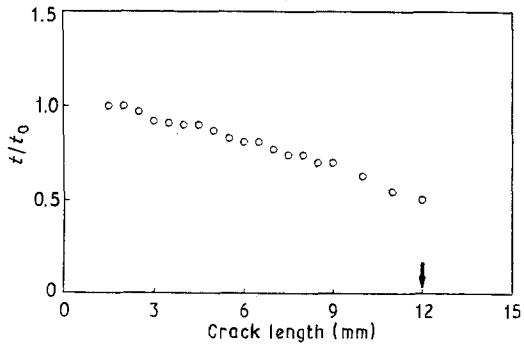

Figure 4 Normalized sample thickness t/t_0 plotted versus the crack length. The vertical arrow indicates the critical crack length.

with the crack length (Fig. 5, regions 1–3). Obviously, this is a direct indication of the progressive increase in the intensity of plastic deformation at the crack tip which resulted in elongation of the grains along the direction of load application (Fig. 5, region 3). In addition to the surface traces, microcracks emanating from the main crack were also observed along the main crack trajectory. Their density progressively increased with the crack depth as shown in Fig. 5, regions 4–6.

The above characterization of the crack tip damage zone showed the shape and the size evolution of that zone with crack length. It also showed the progressive increase in the density of damage features with the crack advance. However, the origin (i.e., dislocation slips and/or twinning) of the surface traces observed has to be identified. In addition, the question, whether there is a phase transformation at the crack tip has to be answered. Therefore, XRD and TEM techniques were used in an attempt to answer these fundamental questions.

3.2. Microstructural origin of damage

Current literature suggests that metastable beta titanium alloys deforms by a mixture of mechanisms involving dislocation slips, twinning and phase transformation [16–20]. Thus, in a previous publication [21] we have employed this information to assume that a similar mixture of mechanisms dominates the damage zone. A transition in the crack propagation behaviour was thus considered due to change in the composition of the dominant damage species. It was noted, in this study however, that the crack propagation undergoes plane strain–plane stress transition at about 6 mm crack length (Figs 1 and 2). This transition is usually associated with the change from brittle-to-ductile behaviour. The importance of this alloy

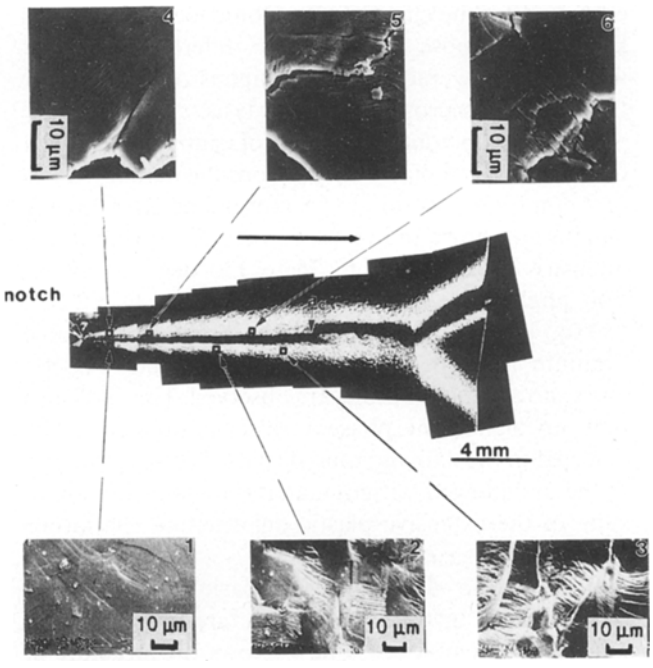

Figure 5 Dark field composite optical micrograph shows the evolution of the damage zone size. The evolution of the surface traces and microcracks densities are also shown.

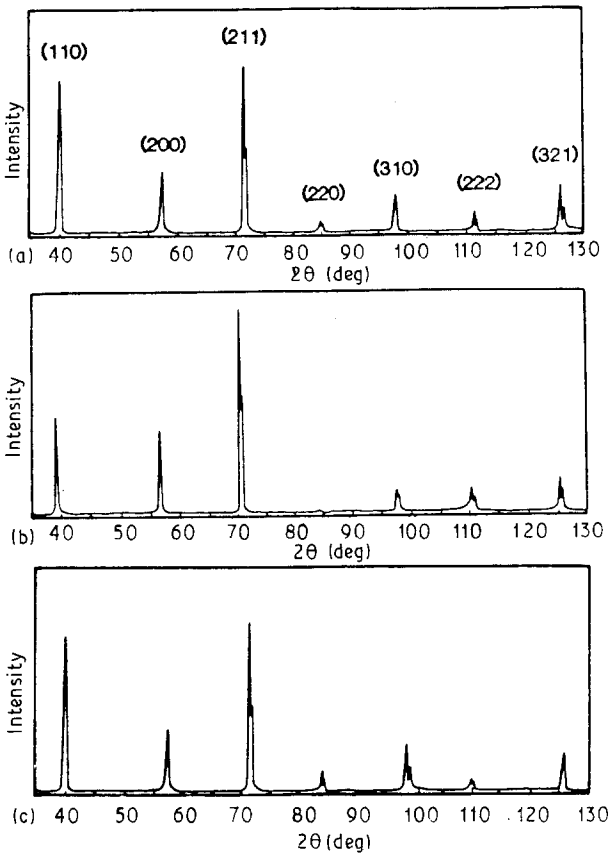

Figure 6 X-ray diffraction of spectra of (a) as-received (undamaged) material, (b) damage zone of 4 mm crack length and (c) damage zone of 8 mm crack length.

and the significance of the phenomena demanded a more detailed examination of the mechanisms involved employing tools of microstructural analysis. This is to ascertain the very nature of the damage species and the manner by which they evolve in response to the change in the crack tip stress state. In addition, the fact that the present knowledge of the deformation mechanisms in this alloy [16–20] is generated under the effect of monotonic loading which is known to impose a stress state different from that imposed by the crack tip. This emphasizes the need for this detailed microstructural analysis.

X-ray diffractometer traces of samples removed from as-received material and from the damage zones of 4 mm (plane strain) and 8 mm (plane stress) crack lengths are shown in Fig. 6a, b and c. X-ray diffraction intensity is scanned from 35 to 130 degs in diffraction angle (2θ). The {1 1 0}, {2 0 0}, {2 1 1}, {2 2 0}, {3 1 0}, {2 2 2} and {3 1 2} of the body centre cubic titanium alloy peaks are shown. In either Fig. 6b and c, no additional peaks are observed. This indicates that no significant phase transformation could be detected in the damage zone. The b c c lattice structure of the undamaged (virgin) material remained intact in spite of the extensive plastic deformation the lattice experienced.

In order to determine the basic origin of the mechanism(s) involved in the fracture process, TEM analysis was employed. Fig. 7 shows the structure of the dislocations in the as-received material. An appreciable density of dislocations is observed. Such a high dislocation density is apparently due to the

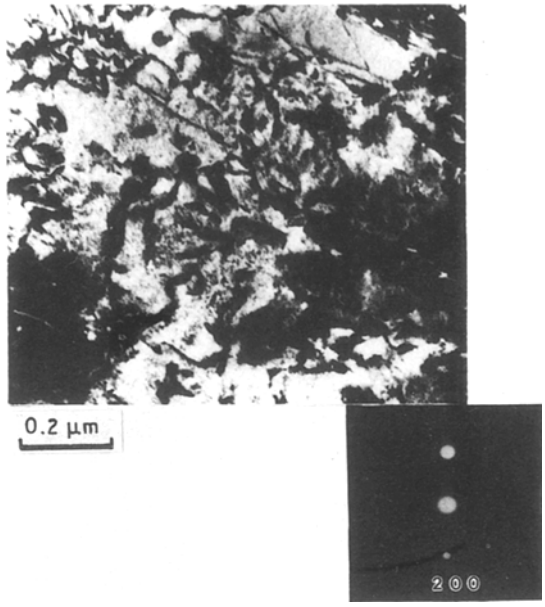

Figure 7 Bright field image of the structure of dislocations in the as-received material.

thermomechanical processes experienced during preparation. The electron diffraction pattern of the as-received material (Fig. 8) indicates a b c c structure. The absence of detectable streaking or distortion in the diffraction spots indicates no lattice distortion [22]. Similarly, samples obtained from the damage zones at 4 mm and 8 mm cracks display no additional diffraction spots, thus suggesting that the b c c structure remained intact during deformation. This implies that neither twinning, nor stress-induced phase transformation were formed within the damage zone. This finding by TEM analysis supports the X-ray data. Additional evidence can also be drawn from the TEM micrographs of the damaged specimens of 4 mm and 8 mm cracks shown in Figs 9 and 10. Nevertheless, the density of dislocations is much higher in the damage zones compared to undeformed specimens. Also, the structure of the dislocations is aligned on $\{1\,\bar{1}\,0\}$ slip

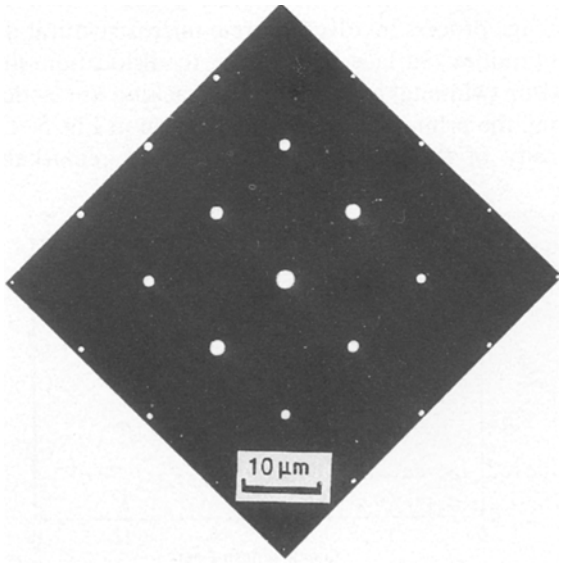

Figure 8 Electron diffraction pattern of as-received material, zone axis $z = [0\,0\,1]$.

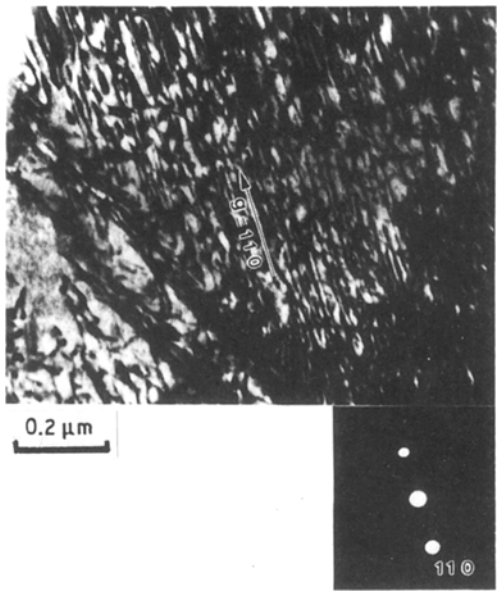

Figure 9 Bright field image of the structure of dislocations in the damage zone of 4 mm crack length.

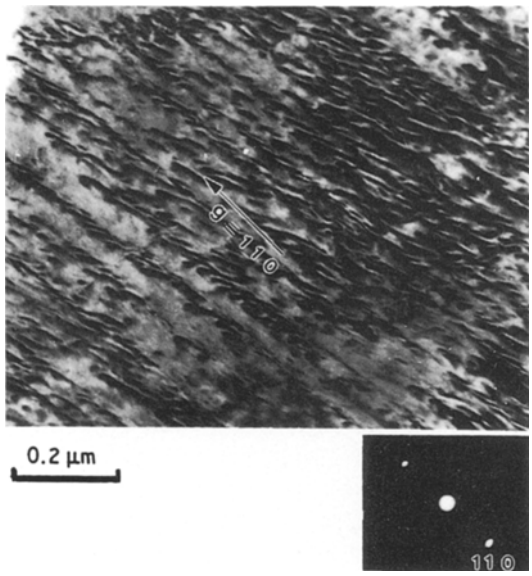

Figure 10 Bright field image of the structure of dislocations in the damage zone of 8 mm crack length.

planes in the damage zones with no evidence of twinning.

The evidence given by X-ray and TEM techniques along with that provided by optical and SEM observation have answered the fundamental question we raised. They clearly indicate that dislocation slips and microcracking are the only damage mechanisms acting at the crack tip in Ti–15–3 alloy. However, it is of interest to know which mechanism is dictating the resistance of the alloy to crack propagation. In other words, which mechanism constitutes a major energy sink and controls the behaviour of crack. This can be achieved by calculating the specific energy of the formation of each mechanism.

3.3. Energy analysis

The total strain energy of dislocations per unit length U can be calculated using the following equation [23]

$$U = \frac{Gb^2}{4\pi}\ln(R/r_0) \quad (1)$$

where G is the shear modulus, R is the outer radius of dislocation, r_0 is the core radius of dislocation and $\boldsymbol{b}$ is the Burger's vector. The shear modulus was approximated as $0.375E$ (where E is the Young's modulus) assuming that Poisson's ratio is 0.35, which is a reasonable approximation for most metals. The value of R was taken as the average half distance between dislocation lines and was found to be equal to 0.01 μm. The core radius of dislocation r_0 was taken to be equal to 0.3 nm. The Burger's vector is equal to one-half of the body diagonal of the b c c unit cell of the present alloy. The lattice parameter a is equal to 0.3263 nm [24].

With all parameters of Equation 1 determined, the value of U is 5.7×10^{-9} N. The density of dislocations was calculated as the total length of dislocations per unit volume. The average thickness of the TEM foil was estimated as 0.1 μm. Figs 9 and 10 were used to measure the average density of dislocations which is about 3.5×10^{15} mm^{-3}. Multiplying the total density of dislocations by U, we obtain the total strain energy of dislocations U_{tot} per unit damage zone volume as 20 MJ m^{-3}.

The specific energy, in J m^{-3}, expended on microcrack formation was also calculated. The density of the microcracks was estimated as the total area created by the microcracks per unit volume in m^2 m^{-3}. The total area of microcracks was approximated by measuring the total length of microcracks and multiplying it by the specimen thickness. The surface energy of Ti is 1.7 J m^{-2} [25]. Accordingly, the total energy expended on microcracking is 4 KJ m^{-3}. This value compared to the energy expended on dislocation slips is obviously negligible. This analysis indicates the minor role of microcracking as a toughening mechanism. More importantly, the low value of the microcracking specific energy compared to that of dislocation slips is concrete evidence that the main energy sink at the crack tip is the dislocation slips.

4. Conclusions

1. Plane strain conditions dominate the initial stage of fatigue crack tip in thin specimens of Ti–15–3. A transition to plane stress is experienced when the plastic zone size exceeds 0.25 of the crack length.

2. Dislocation slips appear to be the sole mechanism of crack tip plasticity. Microcracking near the crack plane occurs as a result of extensive slip damage.

3. The energy of dislocation slips within the plastic zone is three orders of magnitude higher than the energy of microcracking. Thus, it is suggested that the former plays the major role in resisting crack propagation.

References

1. D. GREEN, P. NICHOLSON and J. EMBURY, *J. Amer. Ceram. Soc.* **56** (1973) 619.

2. R. HOAGLAND, J. EMBURY and D. GREEN, *Scripta Metall.* **9** (1975) 907.
3. W. POMPE, H. BAHR, G. GILLE and W. KREHER, *J. Mater. Sci. Lett.* **13** (1978) 2720.
4. M. DOYLE, Ph.D. thesis, Massachusetts Institute of Technology, USA (1971).
5. M. TAKEMORI and R. KAMBOUR, *J. Mater. Sci.* **16** (1981) 1108.
6. P. NEUMAN, *Acta. Metall.* **22** (1974) 1155.
7. *Idem., ibid.* **22** (1974) 1167.
8. J. WEERTMAN, *Phil. Mag.* **43** (1981) 1103.
9. C. LAIRD and G. SMITH, *ibid.* **7** (1962) 847.
10. J. RICE and R. THOMAS, *ibid.* **29** (1974) 73.
11. I. WITTKAMP and E. HORNBOGEN, *Metallograph.* **14** (1977) 237.
12. M. SUGANO and M. GILMORE, *Metall. Trans.* **11A** (1980) 559.
13. I. MOSTAFA, G. WELSCH and A. MOET, submitted to *Intr. J. Frac.* October, 1990.
14. D. BROEK, in "Elementary Engineering Fracture Mechanics" (Martinus Nijhoff, Dordrecht, The Netherlands, 1986) p. 113.
15. R. W. HERTZBERG, in "Deformation and Fracture Mechanics of Engineering Materials" (Wiley, New York, 1976) p. 296.
16. H. ROSENBERGE, *J. Metall,* **35** (1983) 30.
17. Z. LIU, Ph.D. thesis, Case Western Reserve University, USA (1987).
18. G. H. ISAAC and C. HAMMOND, in Proceedings of the 5th International Conference of Titanium, 3, Munich, 1984, edited by G. Lütjering, U. Zwicker and W. Bunk (Deutch Gesellschaft für Metallkunde e.v., 1984) p. 1535.
19. H. M. FLOWER, *ibid.* p. 1651.
20. S. KOMATSU, T. SUGIMOTO, K. KAMEI and T. IBEDA, *ibid.* p. 1575.
21. I. MOSTAFA, G. WELSCH, A. MOET and A. CHUDNOVSKY, *Mater. Sci. and Engin.* **A111** (1989) p. 85.
22. L. E. MURR, in "Electronic and Optical Applications in Materials Science" (McGraw-Hill, New York, 1970) p. 227.
23. D. HULL and D. J. BACON, in "Introduction to Dislocations" (Pergamon, Oxford, 1984) p. 79.
24. M. OKA, C. S. LEE and K. SHIMIZU, *Metall. Trans.* **3** (1972) 37.
25. I. JONES, *Met. Sci. J.* **5** (1971) 15.

Received 3 January
and accepted 18 June 1990